CrossMark
click for updates

# Ab initio and first principles theoretical investigations of triplet–triplet fluorescence in trimethylenemethane biradicals†

Yasunori Matsui,‡[ab] Kosuke Usui,‡[c] Hiroshi Ikeda[ab] and Stephan Irle*[cd]

Theoretical studies on triplet–triplet ($T_1 \rightarrow T_0$) fluorescence of the arylated trimethylenemethane (TMM) biradicals, $^3\mathbf{2}^{\cdot\cdot}$, were carried out using post-Hartree–Fock *ab initio* and various first principles density functional theory methods. Analysis of optimized geometries including bond alternations and spin distributions indicates that the triplet ground ($^3\mathbf{2}^{\cdot\cdot}$) and excited ($^3\mathbf{2}^{\cdot\cdot}*$) states of these biradicals have aromatic and quinoidal characteristics, respectively. Inspection of their calculated electronic structures shows that, in comparison to $^3\mathbf{2}^{\cdot\cdot}$, one of the spins in $^3\mathbf{2}^{\cdot\cdot}*$ is more delocalized onto arene-rings linked to the TMM framework.

The trimethylenemethane[1] (TMM, Fig. 1) biradical is a representative non-Kekulé molecule that has a triplet ground state ($T_0$) owing to its $D_{3h}$ symmetry and pair of degenerate singly-occupied molecular orbitals (SOMOs). As a result of this characteristic, many theoretical and experimental studies have been carried out probing the curious electronic structures and magnetic properties of TMM biradicals.[2] The fact that these biradicals emit triplet–triplet ($T_1 \rightarrow T_0$) fluorescence has received great attention.[3,4]

In previous studies, Matsui, Ikeda, and coworkers described the observation of $T_1 \rightarrow T_0$ fluorescence from the excited states of the 1-methyl-1-phenyl-, 1,1-diphenyl-, and 1-(2-naphthyl)-1-phenyl-substituted TMM biradicals, $^3\mathbf{2a\text{-}c}^{\cdot\cdot}*$ (Scheme 1). For this purpose, thermoluminescence (TL)[5] and two-color two-laser flash photolysis measurements were conducted using the

corresponding aryl-substituted methylenecyclopropanes **1a–c**.[6] Moreover, $T_1 \rightarrow T_0$ fluorescence of these biradicals was utilized as the basis for the design of a new organic light-emitting diode, termed "organic radical light-emitting diode".[5a]

The electronic configurations of the excited $T_1$ states of the TMM biradicals are complicated by their multi-configuration character. Additionally, electronic transition wavelengths and $T_0$ geometries of compound $^3\mathbf{2b}$, computed using time-dependent (TD) density functional theory (DFT)[6] with the B3LYP/cc-pVDZ method, are considerably different from the absorption and emission wavelengths observed experimentally.[7] Thus, more accurate and rigorous *ab initio* quantum chemical studies, and a detailed analysis of geometry relaxation occurring in the $T_1$ state are required to have a greater understanding of the electronic structures of the excited states of TMM biradicals.

In the investigation described below, we carried out a theoretical study of the triplet–triplet fluorescence mechanism to accurately predict structural, electronic and $T_1 \rightarrow T_0$ emission properties of triplet aryl-substituted trimethylenemethane biradicals $^3\mathbf{2}^{\cdot\cdot}*$. *Ab initio* post-Hartree–Fock methods and three
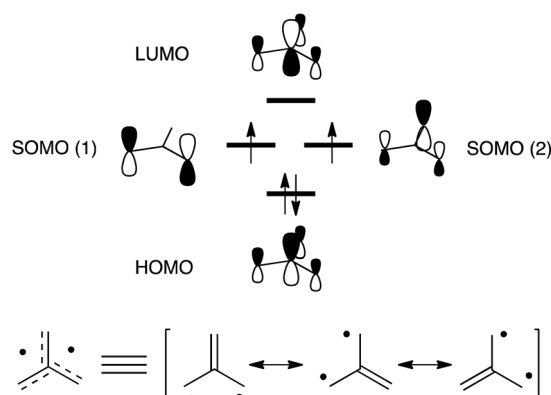
*ᵃDepartment of Applied Chemistry, Graduate School of Engineering, Osaka Prefecture University, Sakai, Osaka 599-8531, Japan*

*ᵇThe Research Institute for Molecular Electronic Devices (RIMED), Osaka Prefecture University, Sakai, Osaka 599-8531, Japan*
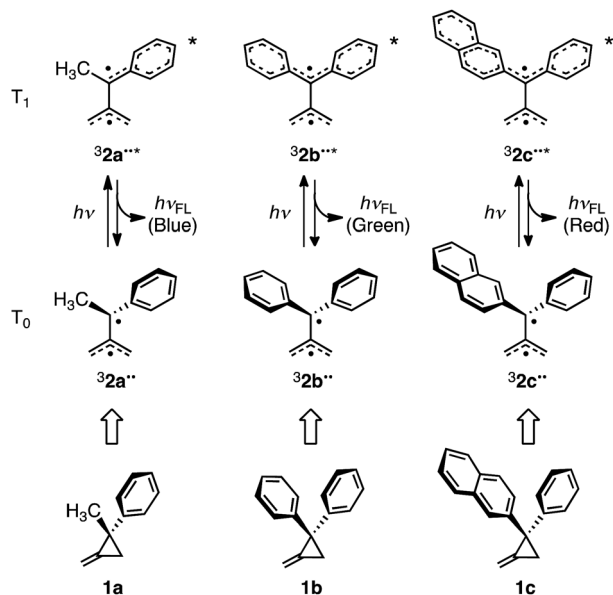
*ᶜDepartment of Chemistry, Graduate School of Science, Nagoya University, Nagoya, 464-8601, Japan. E-mail: sirle@chem.nagoya-u.ac.jp*

*ᵈInstitute of Transformative Bio-Molecules (WPI-ITbM), Nagoya University, Nagoya 464-8601, Japan*

† Electronic supplementary information (ESI) available: Cartesian coordinates of all optimized structures, natural spin densities, natural charges, full citations for ref. 12 and 14. See DOI: 10.1039/c6ra16580j

‡ These authors equally contributed to this work.



Fig. 1 (Top) Frontier molecular orbitals of the parent TMM biradical and (bottom) its corresponding Lewis resonance structures.

**Scheme 1** Chemical structures of **1a**–**c** and electronic structures of $^3$**2a**–**c**$^{\cdot\cdot}$ and $^3$**2a**–**c**$^{\cdot\cdot}$* associated with $T_0$–$T_1$ and $T_1$–$T_0$ transitions accompanying fluorescence.



**Fig. 2** Optimized structures and atom labeling of (left) $^3$**2a**$^{\cdot\cdot}$*, and (center) $^3$**2b**$^{\cdot\cdot}$*, and (right) $^3$**2c**$^{\cdot\cdot}$*. Pink and blue bonds indicate elongated and shortened bonds of $^3$**2**$^{\cdot\cdot}$* relative to $^3$**2**$^{\cdot\cdot}$.

different (TD-)DFT functionals were used for this purpose. When treating open-shell systems, DFT methods often suffer from spin contamination, which usually is more severe when excited rather than ground states are computed. To validate the (TD-)DFT results, high-level *ab initio* benchmark calculations where carried out on $^3$**2**$^{\cdot\cdot}$ and the calculated spin densities and excitation energies obtained by using both types of methods were compared. In this effort, the triplet excited states of three model aryl-substituted TMM biradicals were theoretically studied because they each emit one of the three primary colors (blue, green, and red) (Scheme 1).[5a]

All (TD-)DFT geometry optimizations were performed using the spin-unrestricted UB3LYP, UM06-2X, and CAM-UB3LYP functionals[8] in conjunction with the 6-31G(d) basis set.[9] (TD-)DFT single point energies were obtained using the same methods, however, the larger 6-311+G(d)[9c] basis set was employed. For the smallest, methyl-phenyl substituted biradical, $^3$**2a**$^{\cdot\cdot}$, complete *ab initio* active space self-consistent field (CASSCF)[10] single point energy calculations with 10 $\pi$-orbitals and 10 electrons were performed, followed by a multireference second-order Møller–Plesset perturbation (MRMP2) treatment.[11] All DFT calculations were conducted using Gaussian 09,[12] while the GAMESS-US[13] and MOLPRO[14] program packages were employed for the post-Hartree–Fock calculations. Below, we will refer to $T_1$ and $T_0$ states of **2**$^{\cdot\cdot}$ simply as $^3$**2**$^{\cdot\cdot}$* and $^3$**2**$^{\cdot\cdot}$, respectively.

In the first phase of this study, molecular geometry optimizations were carried out on $^3$**2a**–**c**$^{\cdot\cdot}$ and $^3$**2a**–**c**$^{\cdot\cdot}$* using various DFT functionals.[15] The geometries of triplet ground ($T_0$) and excited ($T_1$) states of these biradicals, obtained by using UB3LYP/6-31G(d), are displayed in Fig. 2, and selected bond lengths are listed in Table 1. The lengths of the C5–C6, C6–C7 and C7–C8 bonds (see Fig. 2 for atom numbering) for $^3$**2a**$^{\cdot\cdot}$ are
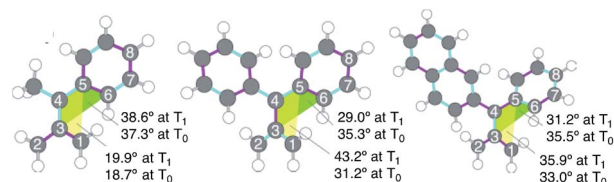
in the range of 1.39–1.42 Å, which is typical for benzene-rings having a small degree of bond alternation. The results of applying a simulated harmonic oscillator model of the aromaticity (HOMA)[16] of the phenyl group in $^3$**2a**$^{\cdot\cdot}$ (0.927) suggests that its aromaticity is relatively high (*i.e.*, roughly equal to that of benzene). In contrast, the respective C5–C6, C6–C7 and C7–C8 bond lengths in $^3$**2a**$^{\cdot\cdot}$* are 1.47, 1.37, and 1.44 Å, suggesting that the degree of bond alternation is higher than in the ground state and, as a result, that the aromatic character of the phenyl group is reduced upon excitation to the $T_1$ state. The greatly lower HOMA value (0.187) calculated for the phenyl group of $^3$**2a**$^{\cdot\cdot}$* also indicates that its aromaticity is strongly reduced.

The changes in the C–C bond lengths taking place in proceeding from the diphenyl-substituted TMM biradical, $^3$**2b**$^{\cdot\cdot}$, to $^3$**2b**$^{\cdot\cdot}$* are similar but somewhat less pronounced in comparison to those seen for the $^3$**2a**$^{\cdot\cdot}$/$^3$**2a**$^{\cdot\cdot}$* system (Table 1). The calculated HOMA value changes are in accord with the reduction of aromaticity taking place in the phenyl group of $^3$**2a**–**b**$^{\cdot\cdot}$ upon electronic excitation, with the largest change occurring in the monophenyl-substituted TMM biradical $^3$**2a**$^{\cdot\cdot}$. On the other hand, the calculated bond lengths and HOMA values for $^3$**2c**$^{\cdot\cdot}$/$^3$**2c**$^{\cdot\cdot}$* deviate from this trend. In this case, the degree of aromaticity of the single phenyl group is less affected by excitation, presumably because excitation is localized mainly in the larger $\pi$-conjugated naphthyl group. The calculated dihedral angles composed of C1–C3–C4–C5 (yellow, Fig. 2) and C3–C4–C5–C6 (green) for the $^3$**2**$^{\cdot\cdot}$/$^3$**2**$^{\cdot\cdot}$* systems also follow these trends.

An analysis of their electronic structures provides further information about the nature of the excited TMM biradicals $^3$**2**$^{\cdot\cdot}$*. Spin distributions of $^3$**2a**–**c**$^{\cdot\cdot}$ and $^3$**2a**–**c**$^{\cdot\cdot}$* at Franck–

**Table 1** Geometry parameters of $^3$**2a**–**c**$^{\cdot\cdot}$ and $^3$**2a**–**c**$^{\cdot\cdot}$* Obtained by using (TD-)UB3LYP/6-31G(d)

| | Bond lengths/Å | | | | | |
|---|---|---|---|---|---|---|
| Biradicals | C3–C4 | C4–C5 | C5–C6 | C6–C7 | C7–C8 | HOMA[a] |
| $^3$**2a**$^{\cdot\cdot}$ | 1.45 | 1.46 | 1.42 | 1.39 | 1.40 | 0.927 |
| $^3$**2a**$^{\cdot\cdot}$* | 1.44 | 1.44 | 1.47 | 1.37 | 1.44 | 0.187 |
| $^3$**2b**$^{\cdot\cdot}$ | 1.47 | 1.47 | 1.42 | 1.39 | 1.40 | 0.929 |
| $^3$**2b**$^{\cdot\cdot}$* | 1.49 | 1.43 | 1.45 | 1.37 | 1.42 | 0.583 |
| $^3$**2c**$^{\cdot\cdot}$ | 1.47 | 1.47 | 1.42 | 1.39 | 1.40 | 0.931 |
| $^3$**2c**$^{\cdot\cdot}$* | 1.47 | 1.45 | 1.39 | 1.42 | 1.40 | 0.896 |

[a] Aromaticity indices of the phenyl group.
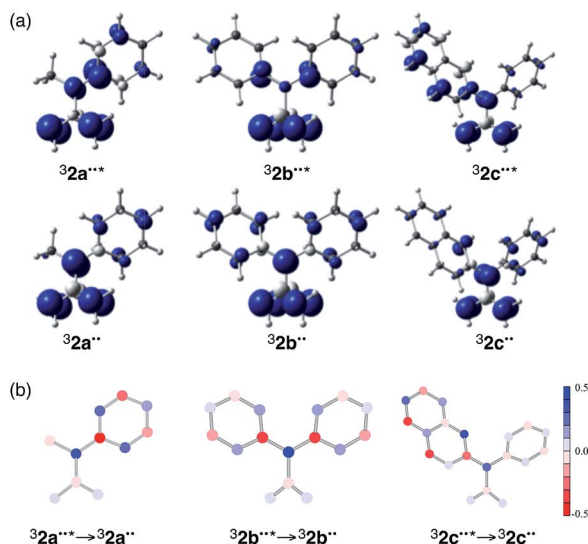
**Fig. 3** (a) Spin distributions for $^3$2a–c$^{\cdot\cdot}$ and $^3$2a–c$^{\cdot\cdot}$* at Franck–Condon geometries. Blue and gray represent positive and negative areas of spin densities, respectively. (b) $T_1$–$T_0$ difference charges occurring in the $^3$2$^{\cdot\cdot}$* → $^3$2$^{\cdot\cdot}$ transitions calculated from natural orbitals for $\alpha$- and $\beta$-spin. Red and blue represent the increase and decrease of $\alpha$-spin density, respectively, upon excitation.

Condon geometries were determined at the (TD-)UB3LYP/6-31G* level of theory (Fig. 3a). The results show that the spin densities of both $^3$2a$^{\cdot\cdot}$ and $^3$2b$^{\cdot\cdot}$ are almost completely localized at C4 (benzylic), C1 (allylic), and C2 (allylic). For $^3$2a–c$^{\cdot\cdot}$, the spin densities at C1 and C2 are almost identical to those of the corresponding ground state, $^3$2a–c$^{\cdot\cdot}$. In contrast, the spin density at C4 of $^3$2a$^{\cdot\cdot}$* is located close to the ipso-position (C5) of the phenyl group. The change taking place in spin densities at each atom in the $^3$2b$^{\cdot\cdot}$ → $^3$2b$^{\cdot\cdot}$* transition is similar to those occurring in the $^3$2a$^{\cdot\cdot}$ → $^3$2a$^{\cdot\cdot}$* transition. Interestingly, the spin density changes caused by the $^3$2c$^{\cdot\cdot}$ → $^3$2c$^{\cdot\cdot}$* transition occur most prominently in the 2-naphthyl group. The alterations in electronic structure are consistent with the geometrical changes that take place in all of the $^3$2$^{\cdot\cdot}$ → $^3$2$^{\cdot\cdot}$* transitions (see the discussion in the previous section).

To express the spin distribution changes that take place in $^3$2$^{\cdot\cdot}$* → $^3$2$^{\cdot\cdot}$ transitions in a quantitative manner, we express

the difference in the spin density of the $i$th atom, $N_i^{T_1-T_0}$ by the equation given in eqn (1),

$$N_i^{T_1-T_0} = \left(\alpha_i^{T_1} - \beta_i^{T_1}\right) - \left(\alpha_i^{T_0} - \beta_i^{T_0}\right) \tag{1}$$

where $\alpha_i^{T_1/T_0}$ and $\beta_i^{T_1/T_0}$ are the respective natural spin densities estimated from $\alpha$ and $\beta$ natural orbitals for $^3$2$^{\cdot\cdot}$* and $^3$2$^{\cdot\cdot}$ (see Tables S7–S9†). Inspection of the data listed in Fig. 3a shows that the spin distributions at C1, C2 and C3 (the allyl moiety) do not significantly change during the $^3$2$^{\cdot\cdot}$* → $^3$2$^{\cdot\cdot}$ transition. Moreover, the sum of their spin densities is approximately 1.1 each for $^3$2a–c$^{\cdot\cdot}$ and $^3$2a–c$^{\cdot\cdot}$* (see Table S10†). Thus, it appears that one unpaired electron is delocalized over the allyl moieties of both $^3$2a–c$^{\cdot\cdot}$ and $^3$2a–c$^{\cdot\cdot}$*. The other unpaired electron in the $T_1$ excited state ($^3$2$^{\cdot\cdot}$*) is delocalized over the remainder of the molecule, whereas it is localized on C4 in $^3$2a–c$^{\cdot\cdot}$. The electronic structure change occurring upon excitation is also made apparent by inspection of the flow of spin density from C4 to C5 (Fig. 3b). The excitation-promoted, spin density reorganization decreases on proceeding from $^3$2a$^{\cdot\cdot}$ to $^3$2c$^{\cdot\cdot}$. In addition, introduction of benzene or naphthalene rings leads to an enhancement in electron delocalization in the $T_0$ state (Tables S7–S9†). The analysis presented above indicates that electronic structures of $^3$2a–c$^{\cdot\cdot}$ and $^3$2a–c$^{\cdot\cdot}$* can be schematically depicted in the manner shown in Scheme 1. As a result, the distribution of the second unpaired electron is controlled by introduction of aromatic groups on the TMM biradical backbone (e.g., $^3$2c$^{\cdot\cdot}$).

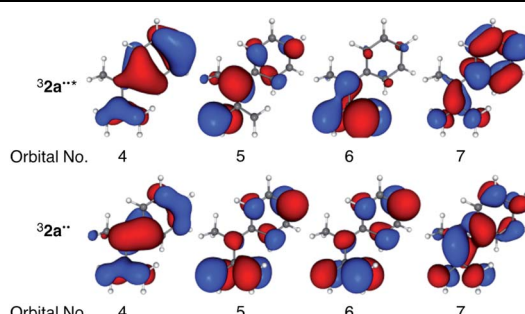Previously, Ikeda and co-workers experimentally determined the wavelength maxima for $T_1$ → $T_0$ fluorescence of $^3$2$^{\cdot\cdot}$* by using TL methods.[5a] The TL maxima of $^3$2a$^{\cdot\cdot}$*, $^3$2b$^{\cdot\cdot}$* and $^3$2c$^{\cdot\cdot}$* in methylcyclohexane matrices at ca. 130 K are 451, 501, and 602 nm, respectively. In the present work, we calculated the fluorescence wavelengths of $^3$2a–c$^{\cdot\cdot}$* using various TD-DFT functionals (Table 2). Interestingly, the fluorescence wavelengths obtained by using the UB3LYP method match well with the experimentally determined values.[5] Although use of the UM06-2X method also gives maxima that are close to the experimental values, it slightly overestimates the excitation energies. Utilization of the long-range corrected CAM-UB3LYP functional does not lead to improved results, suggesting that charge-transfer interactions are not important in $^3$2$^{\cdot\cdot}$*. The use of UHF in this functional for treatment of large electronic separations suffers from a more serious spin contamination ($\langle S^2 \rangle$ ~2.54–4.01), especially in the case of $^3$2c$^{\cdot\cdot}$.

**Table 2** Fluorescence wavelength maxima ($\lambda_{Em}$) and oscillator strengths (f) of TMM biradicals obtained by experimental and various TD-DFT methods

| | Exp[a] | | TD-DFT[b] | |
| | TL | UB3LYP | UM06-2X | CAM-UB3LYP |
| Biradical | $\lambda_{TL}$/nm | $\lambda_{Em}$/nm ($\langle S^2 \rangle$, f) | $\lambda_{Em}$/nm ($\langle S^2 \rangle$, f) | $\lambda_{Em}$/nm ($\langle S^2 \rangle$, f) |
|---|---|---|---|---|
| $^3$2a$^{\cdot\cdot}$ | 451 | 443 (2.43, 0.003) | 438 (2.28, 0.005) | 440 (3.10, 0.001) |
| $^3$2b$^{\cdot\cdot}$ | 501 | 479 (2.24, 0.010) | 464 (2.23, 0.018) | 443 (2.54, 0.007) |
| $^3$2c$^{\cdot\cdot}$ | 602 | 613 (2.63, 0.002) | 554 (2.39, 0.004) | 903 (4.01, 0.000) |

[a] From ref. 5a. [b] The 6-311+G(d) and 6-31G(d) basis sets were employed for single point calculations and optimizations, respectively.

**Table 3** NOON Values of $^3$2a$^{\cdot\cdot}$ and $^3$2a$^{\cdot\cdot}$* obtained using CASSCF(10o, 10e) calculations



| NOON | Orbital no. | 1 | 2 | 3 | 4 | 5 | 6 | 7 | 8 | 9 | 10 |
|---|---|---|---|---|---|---|---|---|---|---|---|
| | $^3$2a$^{\cdot\cdot}$* | 1.92 | 1.90 | 1.88 | 1.47 | 1.02 | 0.97 | 0.55 | 0.12 | 0.09 | 0.07 |
| | 2a$^{\cdot\cdot}$ | 1.96 | 1.92 | 1.90 | 1.87 | 1.00 | 1.00 | 0.13 | 0.10 | 0.08 | 0.04 |

To validate the (TD-)DFT results presented above, the electronic configuration of $^3$2a$^{\cdot\cdot}$* was evaluated by employing post-Hartree–Fock CASSCF and multireference MP2 calculations. First, 10 π-orbitals of $^3$2a$^{\cdot\cdot}$ were obtained using the RHF/6-311+G(d) method for the singlet spin state. Subsequent CASSCF calculations were carried out using a full π-orbital (10e, 10o) active space for the triplet ground state. In Table 3 are listed the corresponding natural orbital occupation numbers (NOON), where 2, 1, and 0 indicates doubly-, singly-, and un-occupied orbitals, respectively. Importantly, a deviation of NOON from integer numbers implies that the wavefunction has multireference character.[17] Analysis of the NOON values for $^3$2a$^{\cdot\cdot}$ indicates the existence of four doubly-occupied (NOON > 1.87), two singly-occupied (NOON ∼ 1.00), and four un-occupied (NOON < 0.13) orbitals within the active space. On the other hand, the NOON values of orbitals numbers 4 and 7 in $^3$2a$^{\cdot\cdot}$* deviate largely from integer values, signaling that the wavefunction has multireference character. Except for natural orbitals 4–7, the NOON values and orbital shapes of $^3$2a$^{\cdot\cdot}$* and $^3$2a$^{\cdot\cdot}$ are almost identical. The singly-occupied natural orbital of $^3$2a$^{\cdot\cdot}$ is localized on the TMM moiety, while singly occupied natural orbitals of $^3$2a$^{\cdot\cdot}$* (Table 3) are delocalized on the phenyl group. The fact that this finding is consistent with the natural charge distributions obtained by using (TD-)DFT calculations (Fig. 3) validates the DFT-based results.

The CASSCF-determined emission energy of the benchmark model $^3$2a$^{\cdot\cdot}$ is 2.62 eV (473 nm) and that arising from MRMP2 is 2.51 eV (495 nm). The MRMP2 result is in good agreement with that determined experimentally (2.74 eV, 451 nm), and the TD-DFT determined emission energy (2.82 eV, 440 nm) is also close to the experimental value. These findings suggest that a well-balanced use of dynamic and non-dynamic correlations is necessary for quantitatively accurate assessment of the emission wavelengths of $^3$2$^{\cdot\cdot}$*. The somewhat surprising similarity of the MRMP2 and UB3LYP results show that conceptually more simple density functional approaches can be applied to the complex electronic and molecular structures of $^3$2$^{\cdot\cdot}$*. This is most likely a consequence of fortuitous error compensations.

In conclusion, studies aimed at understanding the T$_1$–T$_0$ fluorescence of aryl-substituted TMM biradicals $^3$2$^{\cdot\cdot}$* were carried out using quantum chemical calculations. The results of calculations using high-level *ab initio* and various DFT functionals reveal that the wavefunctions of $^3$2$^{\cdot\cdot}$* possesses significant multireference character. However, use of DFT approaches with sufficiently large basis sets leads to predictions of reasonable emission wavelengths of $^3$2$^{\cdot\cdot}$*. In addition, the calculated changes of bond lengths and spin distributions demonstrate that significant relaxation of molecular geometries occurs in T$_1$ on going from an aromatic ground state to quinoid structured excited state. The overall results of this work demonstrate that it is possible to use DFT-based methods to estimate accurately the fluorescence properties of organic open-shell species.[18] This ability should accelerate the development and application of luminescent radical materials.

## Acknowledgements

## Notes and references

1 (*a*) P. Dowd, *Acc. Chem. Res.*, 1972, **5**, 242–248; (*b*) J. A. Berson, *Acc. Chem. Res.*, 1978, **11**, 446–453; (*c*) M. Abe, *Chem. Rev.*, 2013, **113**, 7011–7088.

2 L. V. Slipchenko and A. I. Krylov, *J. Chem. Phys.*, 2003, **118**, 6874–6883.

3 (a) J. A. Berson, R. J. Bushby, J. M. McBride and M. Tremelling, *J. Am. Chem. Soc.*, 1971, **93**, 1544–1546; (b) M. S. Platz, J. M. McBride, R. D. Little, J. J. Harrison, A. Shaw, S. E. Potter and J. A. Berson, *J. Am. Chem. Soc.*, 1976, **98**, 5725–5726; (c) N. J. Turro, M. J. Mirbach, N. Harrit, J. A. Berson and M. S. Platz, *J. Am. Chem. Soc.*, 1978, **100**, 7653–7658.

4 H. Ikeda, H. Namai, H. Taki and T. Miyashi, *J. Org. Chem.*, 2005, **70**, 3806–3813.

5 (a) H. Namai, H. Ikeda, Y. Hoshi, N. Kato, Y. Morishita and K. Mizuno, *J. Am. Chem. Soc.*, 2007, **129**, 9032–9036; (b) H. Ikeda, Y. Matsui, I. Akimoto and K. Kan'no, *Aust. J. Chem.*, 2010, **63**, 1342–1347; (c) Y. Matsui, H. Namai, I. Akimoto, K. Kan'no, K. Mizuno and H. Ikeda, *Tetrahedron*, 2011, **67**, 7431–7439.

6 (a) P. Hohenberg and W. Kohn, *Phys. Rev.*, 1964, **136**, B864–B871; (b) W. Kohn and L. J. Sham, *Phys. Rev.*, 1965, **140**, A1133–A1138; (c) R. Bauernschmitt and R. Ahlrichs, *Chem. Phys. Lett.*, 1996, **256**, 454–464; (d) M. E. Casida, C. Jamorski, K. C. Casida and D. R. Salahub, *J. Chem. Phys.*, 1998, **108**, 4439–4449; (e) R. E. Stratmann, G. E. Scuseria and M. J. Frisch, *J. Chem. Phys.*, 1998, **109**, 8218–8224.

7 (a) Y. Matsui, T. Kido, E. Ohta and H. Ikeda, *Chem. Commun.*, 2014, **50**, 13963–13966; (b) Y. Matsui, D. Kawahara, E. Ohta and H. Ikeda, *Phys. Chem. Chem. Phys.*, 2013, **15**, 7064–7069.

8 (a) Y. Zhao and D. Truhlar, *Theor. Chem. Acc.*, 2008, **120**, 215–241; (b) C. Lee, W. Yang and R. G. Parr, *Phys. Rev. B: Condens. Matter Mater. Phys.*, 1988, **37**, 785–789; (c) A. D. Becke, *J. Chem. Phys.*, 1993, **98**, 5648–5652; (d) T. Yanai, D. P. Tew and N. C. Handy, *Chem. Phys. Lett.*, 2004, **393**, 51–57.

9 (a) P. C. Hariharan and J. A. Pople, *Theor. Chem. Acc.*, 1973, **28**, 213–222; (b) W. J. Hehre, R. Ditchfield and J. A. Pople,

*J. Chem. Phys.*, 1972, **56**, 2257–2261; (c) R. Krishnan, J. S. Binkley, R. Seeger and J. A. Pople, *J. Chem. Phys.*, 1980, **72**, 650–654.

10 B. O. Roos, *Adv. Chem. Phys.*, 1987, **69**, 399–446.

11 (a) K. Hirao, *Chem. Phys. Lett.*, 1992, **190**, 374–380; (b) K. Hirao, *Chem. Phys. Lett.*, 1992, **196**, 397–403; (c) K. Hirao, *Chem. Phys. Lett.*, 1993, **201**, 59–66.

12 M. J. Frisch, *et al.*, *Gaussian 09, Revision C.01*, Gaussian, Inc., Wallingford, CT, 2009.

13 M. W. Schmidt, K. K. Baldridge, J. A Boatz, S. T. Elbert, M. S. Gordon, J. J. Jensen, S. Koseki, N. Matsunaga, K. A. Nguyen, S. J. Su, T. L. Windus, M. Dupuis and J. A. Montgomery Jr, *J. Comput. Chem.*, 1993, **14**, 1347–1363.

14 H. J. Werner, *et al.*, MOLPRO, version 2010, a package of *ab initio* programs; see http://www.molpro.net.

15 For the details, see the ESI.†

16 HOMA is an index of aromaticity obtained by considering bond lengths of phenyl-rings. HOMA values close to 1 and 0 indicate high and low aromaticity, respectively. See: J. Kruszewskia and T. M. Krygowski, *Tetrahedron Lett.*, 1972, **13**, 3839–3842.

17 S. Yamanaka and K. Yamaguchi, *Bull. Chem. Soc. Jpn.*, 2004, **77**, 1269–1286.

18 (a) H. Namai, H. Ikeda, Y. Hoshi and K. Mizuno, *Angew. Chem., Int. Ed.*, 2007, **46**, 7396–7398; (b) Y. Hattori, T. Kusamoto and H. Nishihara, *Angew. Chem., Int. Ed.*, 2015, **54**, 3731–3734; (c) Y. Hattori, T. Kusamoto and H. Nishihara, *Angew. Chem., Int. Ed.*, 2014, **53**, 11845–11848; (d) Q. Peng, A. Obolda, M. Zhang and F. Li, *Angew. Chem., Int. Ed.*, 2015, **54**, 7091–7095.